Mean curvature flow for generating discrete surfaces with piecewise constant mean curvatures

AUTHOR(S):

Hayashi, Kazuki; Jikumaru, Yoshiki; Ohsaki, Makoto; Kagaya, Takashi; Yokosuka, Yohei

CITATION:

Hayashi, Kazuki ...[et al]. Mean curvature flow for generating discrete surfaces with piecewise constant mean curvatures. Computer Aided Geometric Design 2023, 101: 102169.

ISSUE DATE:

2023-04

URL:

http://hdl.handle.net/2433/282816

Computer Aided Geometric Design 101 (2023) 102169

Contents lists available at ScienceDirect

Computer Aided Geometric Design

journal homepage: www.elsevier.com/locate/cagd

Mean curvature flow for generating discrete surfaces with piecewise constant mean curvatures ☆

Kazuki Hayashi [a,*], Yoshiki Jikumaru [b], Makoto Ohsaki [a], Takashi Kagaya [c], Yohei Yokosuka [d]

[a] Department of Architecture and Architectural Engineering, Kyoto University, Japan
[b] Institute of Mathematics for Industry, Kyushu University, Japan
[c] Department of Sciences and Informatics, Muroran Institute of Technology, Japan
[d] Department of Architecture and Architectural Engineering, Kagoshima University, Japan

ARTICLE INFO

Article history:
Received 27 March 2022
Received in revised form 3 January 2023
Accepted 10 January 2023
Available online 24 January 2023

Keywords:
Form-finding
Discrete differential geometry
Constant mean curvature (CMC)
Mean curvature flow
Energy minimization

ABSTRACT

Piecewise constant mean curvature (P-CMC) surfaces are generated using the mean curvature flow (MCF). As an extension of the known fact that a CMC surface is the stationary point of an energy functional, a P-CMC surface can be obtained as the stationary point of an energy functional of multiple patch surfaces and auxiliary surfaces between them. A new formulation is presented for the MCF as the negative gradient flow of the energy functional for multiple patch continuous surfaces, which are further discretized so as to determine the change in the vertex positions of triangular meshes on the surface as well as along the internal boundaries between patches. Numerical examples show that multiple patch surfaces approximately reach the specified mean curvatures through the proposed method, which can diversify the options for the shape design using CMC surfaces.

1. Introduction

With the development of computer-based analysis technology and the diversification of feasible architectural forms, many attempts have been made to design shell structures with complex shapes. Free-form surfaces such as Bézier, B-spline and NURBS surfaces are frequently used to parametrically determine the shapes of complex surfaces (Farin, 2001). The shape of a free-form surface can be interactively adjusted by varying locations of control points to meet various design needs. Numerous optimization methods for free-form surfaces have also been proposed to obtain reasonable shapes in terms of structural performance and constructional efficiency (Kimura and Ohmori, 2008; Cui and Ohsaki, 2018; Gao et al., 2019). Besides, isogeometric analysis approaches have been proposed in which parametric expressions can be directly applied to represent the models for simulation of structural performances (Cottrell et al., 2009).

While there are surface classes such as Bézier and NURBS whose shapes are determined by control points, there are also surface classes whose shapes are determined by specifying boundary conditions and geometric invariants, e.g., mean curvature and Gaussian curvature. More complex invariants that are functions of curvatures, gradient, metric tensor, etc., can be used for characterizing the surface shape (Fujita and Ohsaki, 2010). In particular, the constant mean curvature (CMC) surfaces are uniquely determined by specifying the boundary shape and the mean curvature. Soap films and bubbles are

☆ Editor: Wenping Wang.
* Corresponding author.
E-mail address: hayashi.kazuki@archi.kyoto-u.ac.jp (K. Hayashi).

https://doi.org/10.1016/j.cagd.2023.102169

widely known as examples of CMC surfaces that exist in nature. Surface with zero mean curvature is specifically called minimal surface and has been studied since the 18th century with the development of variational principles (Meeks and Pérez, 2011).

The evolution of surfaces by mean curvature is studied from the late 1970s (Brakke, 1978). Huisken (1984) proposed a method to change surface shapes using the normal vector and mean curvature, and called it "flow by mean curvature", which is later widely recognized as mean curvature flow (MCF), and has been extensively studied as a method of smoothing the surface shape (Desbrun et al., 1999; Schneider and Kobbelt, 2001). However, most of the studies on CMC surfaces and MCF do not consider boundary conditions. In the field of structural shape optimization, derivatives of functional with respect to boundary perturbation of surface are computed using the formulations of material derivatives (Zolésio, 1981; Arora et al., 1992). The variation of surface integral is transformed to those on the surface and along the boundary.

There are also various examples of using CMC surfaces in the fields of architecture and civil engineering. Since the minimal surface can be at equilibrium by a uniform membrane stress, it is utilized in form-finding methods to obtain reasonable shapes of tensile structures (Lewis and Gosling, 1993). Similarly, CMC surfaces are known to satisfy equilibrium conditions by uniform tensile stress against a uniform normal loading condition, or a constant pressure, and approximating the structural shape to a CMC surface is expected to enhance structural performance of pneumatic membrane structure. Furthermore, since CMC surfaces enclose the specified volume bounded by the boundary region and the surface itself with the minimum area, the architectural shape designed using CMC surfaces can save the material cost for the construction.

However, as pointed out by the authors (Hayashi et al., 2021), despite the fact that continuous surfaces are often converted to discrete surfaces such as triangular meshes during structural analysis and construction phases, there are relatively few architectural design methods that directly handle discrete surfaces (Tellier et al., 2018). Polthier and Rossman (2002) also pointed out that discrete CMC surfaces are less available compared to continuous ones. In addition, most previous studies connecting multiple CMC surfaces are limited to the case where a single pattern is periodically arranged (Thomas et al., 1988; Cao et al., 2016). In order to generate various architectural shapes, it is desirable to combine different CMC surfaces so that they are C^0 continuous, which is to be called piecewise CMC (P-CMC) surface, instead of using a single CMC surface. Although Pinkall and Polthier (1993) successfully generated minimal surfaces for triangular meshes in which some edges are shared by three triangular elements, i.e., the patches are C^0 continuous at the edges, the applicability to non-zero CMC surfaces is not verified. In fact, although they are not CMC surfaces, there are a number of construction examples of building roofs that have continuous C^0 internal boundaries by stiffening them with beams or cables (Burger and Billington, 2006; Michiels et al., 2016). Considering the above background, formulating the method for generating P-CMC surface within the framework of discrete differential geometry is of great engineering significance. Furthermore, a method based on minimization of a functional has practical importance because various sophisticated optimization algorithms can be utilized.

In this study, we derive the MCF from the variational principle of the energy functional of surfaces for the purpose of generating discrete P-CMC surfaces. Although several studies have formulated gradient flows that change the surface shape to minimize the energy functional for achieving CMC (Pan et al., 2012; Crane et al., 2013; Yu et al., 2015), they treat single, simple or closed surfaces. On the other hand, this research is distinguished from the previous studies in the following aspects;

1. Multiple, complex, and non-closed patch surfaces are simultaneously handled to achieve P-CMC.
2. Auxiliary surfaces are introduced at the internal boundary and their energy is integrated.
3. The internal boundary that is equilibrium in its perpendicular direction is also automatically determined based on the variational principle.
4. Unlike the volume-preserving mean curvature flow of Surface Evolver (Brakke, 1992), the proposed method allows generating P-CMC surfaces with specified mean curvatures by encapsulating the volume to the objective function and representing the energy gradient explicitly on stationary points.

This paper is organized as follows. In Sec. 2, the basics of generating CMC surfaces using MCFs are explained first, a method of generating P-CMC surfaces is formulated based on the conventional MCF, and a discretized form of the proposed formulation is presented. In Sec. 3, the implementation details such as the overall workflow, line search, Nesterov momentum and their hyper-parameter setting are presented. In Sec. 4, numerical examples are provided to demonstrate applicability of the proposed method for generating various P-CMC surfaces. Section 5 is a concluding remark that summarizes the formulation of the proposed method and findings in this paper.

2. Discrete mean curvature flow for generating piecewise constant mean curvature surfaces

2.1. Continuous mean curvature flow without boundaries

In this section, the basics of generating CMC surfaces using MCFs are explained for completeness of the paper. Although the contents in this section are already presented in the literature such as Refs. (Mantegazza, 2011; López, 2013), presenting the basic concepts of MCF would be helpful for understanding our formulation which will be explained in Sec. 2.2.

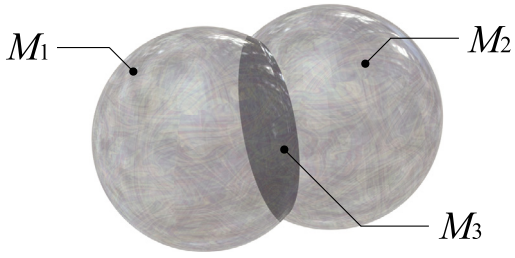

Fig. 1. CG image of a double bubble.

A typical energy functional of an arbitrary closed surface M is formulated as, using a constant α,

$$\tilde{E} = \alpha A - V \tag{1}$$

where V is the volume enclosed by the closed surface M and A is the surface area. For a perturbed surface with a velocity vector field $\mathbf{v}$, the first variation of the energy functional can be calculated as

$$\delta\tilde{E}(\mathbf{v}) = -\int_M \mathbf{v}\cdot(1+2\alpha H)\boldsymbol{\nu} dA \tag{2}$$

where H is the mean curvature of the closed surface M and its sign is chosen so that H is negative for convex surfaces, and $\boldsymbol{\nu}$ is the outer pointing unit normal vector. The formula thus implies that the stationary point of the energy functional is the CMC surface with the mean curvature $H = -1/(2\alpha)$, and a time depending family of closed surfaces may converge to the CMC when the closed surface moves along the direction of the negative gradient, which is so-called MCF. Equation (2) also implies that the CMC surface can be at equilibrium with uniform tension α against unit internal pressure.

2.2. Continuous mean curvature flow considering internal boundaries

One of the most familiar examples of P-CMC surfaces might be bubbles. Fig. 1 illustrates a typical example of a double bubble: a pair of spherical surfaces sticking together to create an internal circular boundary surface between them.

The method proposed in this study is strongly inspired by this natural phenomenon. The MCF for this P-CMC surface can be formulated as follows. Let M_1 and M_2 be surfaces corresponding to each external bubble surface and M_3 be a surface corresponding to the internal boundary between the external bubbles as shown in Fig. 1. The intersection curve of all surfaces is denoted by Γ. Using arbitrary constants α_1, α_2 and α_3, the energy functional can be expanded as

$$\tilde{E} = \sum_{i=1}^{3}(\alpha_i A_i) - V \tag{3}$$

where V is the volume enclosed by the surfaces M_1 and M_2, and A_i is the surface area of M_i for $i = 1, 2, 3$. Denoting by $\mathbf{n}_i$ the co-normal vector of the surface M_i for $i = 1, 2, 3$ on the intersection curve Γ, the first variation of the surface area A_i and the volume V for a perturbed double bubble type surface with a velocity $\mathbf{v}$ can be formulated as

$$\begin{aligned}\delta A_i(\mathbf{v}) &= \int_{M_i} \mathrm{div}_{M_i}\mathbf{v} dA \\ &= -\int_{M_i} \mathbf{v}\cdot 2H_i\boldsymbol{\nu}_i dA + \int_\Gamma \mathbf{v}\cdot\mathbf{n}_i ds\end{aligned} \tag{4}$$

for $i = 1, 2, 3$ and

$$\delta V(\mathbf{v}) = \sum_{i=1}^{2}\int_{M_i}\mathbf{v}\cdot\boldsymbol{\nu}_i dA \tag{5}$$

where div_{M_i} is the divergence on the surface M_i. Equations (4) and (5) thus imply that

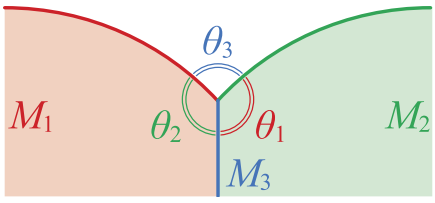

Fig. 2. Contact angle condition.

$$\begin{aligned}\delta\tilde{E}(\mathbf{v}) = &-\sum_{i=1}^{2}\int_{M_i}\mathbf{v}\cdot(1+2\alpha_i H_i)\boldsymbol{\nu}_i dA\\ &-\int_{M_3}\mathbf{v}\cdot(2\alpha_3 H_3)\boldsymbol{\nu}_3 dA\\ &+\int_{\Gamma}\mathbf{v}\cdot\sum_{i=1}^{3}(\alpha_i\mathbf{n}_i)ds\end{aligned} \tag{6}$$

which yields that the surface obtained as the stationary point of the energy functional satisfies the following conditions:

- CMC condition: Each surface is a CMC surface with the mean curvature $H_1 = -1/(2\alpha_1)$ on M_1, $H_2 = -1/(2\alpha_2)$ on M_2, and $H_3 = 0$ on M_3.
- Contact angle condition: The surface satisfies contact angle condition

$$\frac{\sin\theta_1}{\alpha_1} = \frac{\sin\theta_2}{\alpha_2} = \frac{\sin\theta_3}{\alpha_3} \tag{7}$$

on the intersection curve Γ, where $\theta_i \in (0,\pi)$ is the angle between surfaces M_j and M_k for $i, j, k \in 1, 2, 3$, as illustrated in Fig. 2.

Because α_i is the uniform tensile force under constant unit pressure, Eq. (7) corresponds to equilibrium along the internal boundary Γ. For example, the first equality is written as $\alpha_2 \sin\theta_1 = \alpha_1 \sin\theta_2$, which is the equilibrium equation in the perpendicular direction of M_3.

If a time depending family of double bubble type surfaces satisfies the contact angle condition, the gradient of the energy functional is well-defined and we can evolve the surface to a negative gradient orientation to converge to the stationary point of the energy functional.

This study aims to construct the surface with specified CMCs and boundary shape, and the above variational calculations can be applied even if we specify the boundary shape of M_1 and M_2 except the intersection curve Γ as follows. Let the exterior surfaces M_1, M_2 and the internal surface M_3 satisfy the following conditions:

- M_1, M_2 and M_3 generate the triple junction on the intersection curve Γ.
- Γ_1 and Γ_2 are respectively the specified boundary segments of M_1 and M_2 except Γ, namely, $\partial M_i = \Gamma \cup \Gamma_i$ and Γ_i is fixed for $i = 1, 2$.
- A surface Π is chosen to pass through the curves Γ_1 and Γ_2.
- A boundary segment $\Gamma_3 := \partial M_3 \setminus \Gamma$ can move freely on Π.

A typical choice of Γ_1, Γ_2 and Π is that Π is a plane and $\Gamma_1 \cup \Gamma_2$ is a planar curve on Π as shown in Fig. 3. We define V in Eq. (3) as the volume enclosed by M_1, M_2 and Π for the specified boundary shape problem. For arbitrary velocity $\mathbf{v}$ of perturbed double bubble type surface satisfying the conditions above, $\mathbf{v} = \mathbf{0}$ holds on $\Gamma_1 \cup \Gamma_2$ and $\mathbf{v}$ is parallel to Π on Γ_3, and the first variation of the energy functional $\tilde{E}$ for the perturbation can be calculated as

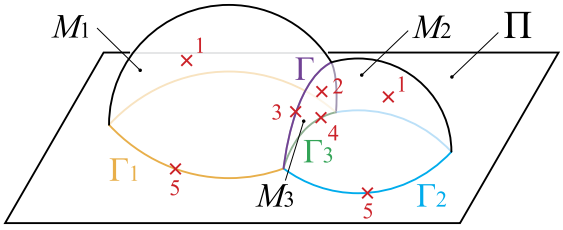

Fig. 3. Typical example of two exterior surfaces (M_1, M_2) and one interior surface (M_3) bounded by a plane (Π).

$$\begin{aligned}\delta\tilde{E}(\mathbf{v}) = &-\sum_{i=1}^{2}\int_{M_i}\mathbf{v}\cdot(1+2\alpha_i H_i)\boldsymbol{\nu}_i dA\\ &-\int_{M_3}\mathbf{v}\cdot(2\alpha_3 H_3)\boldsymbol{\nu}_3 dA\\ &+\int_{\Gamma}\mathbf{v}\cdot\sum_{i=1}^{3}(\alpha_i\mathbf{n}_i)ds+\int_{\Gamma_3}\mathbf{v}\cdot(\alpha_3\mathbf{n}_3)ds\end{aligned} \tag{8}$$

Therefore, the stationary point of $\tilde{E}$ satisfies, in addition to the CMC condition and the contact angle condition,

- Orthogonal condition (Neumann boundary condition): Γ_3 is on Π and M_3 is perpendicular to Π on Γ_3

and the following condition obviously holds from the settings of the double bubble type surface:

- Fixed boundary condition (Dirichlet boundary condition): $\partial M_i \setminus \Gamma$ coincides with the specified boundary segment Γ_i for $i = 1, 2$.

The MCF can thus be derived as the negative gradient flow of $\tilde{E}$ for a family of double bubble type surfaces satisfying the contact angle condition, the orthogonal condition and the fixed boundary condition.

2.3. Discretized form of Sec. 2.2

The discretized form of the MCF is formulated in this section to apply the MCF to triangular meshes. Let Π be the (X, Y)-plane in the 3-dimensional space with the coordinates (X, Y, Z), and consider triangulated surfaces M_1 and M_2 which contact with the plane Π as shown in Fig. 3. We consider an auxiliary internal surface M_3 whose boundary lies on $\Gamma = M_1 \cap M_2$ and Π. For each oriented triangle $T = (p, q_j, q_{j+1})$ of the surface M_i for $i = 1, 2, 3$, we define the area $A(T)$ and the unit normal vector $\boldsymbol{\nu}_T$ as follows:

$$A(T) = \frac{1}{2}\|(\mathbf{q}_j - \mathbf{p}) \times (\mathbf{q}_{j+1} - \mathbf{p})\| \tag{9a}$$

$$\boldsymbol{\nu}_T = \frac{(\mathbf{q}_j - \mathbf{p}) \times (\mathbf{q}_{j+1} - \mathbf{p})}{\|(\mathbf{q}_j - \mathbf{p}) \times (\mathbf{q}_{j+1} - \mathbf{p})\|} \tag{9b}$$

where the values expressed in bold font are their position vectors. Then we define the area A_i for the surface M_i and the volume V bounded by the surfaces M_1, M_2 and the plane Π as follows:

$$A_i = \sum_{T\in M_i} A(T), \quad i = 1, 2, 3 \tag{10a}$$

$$V = \frac{1}{6}\sum_{T=(p,q_j,q_{j+1})\in M_1\cup M_2}\langle\mathbf{p}, \mathbf{q}_j \times \mathbf{q}_{j+1}\rangle \tag{10b}$$

The function E is regarded as the discretized form of the functional $\tilde{E}$ in the smooth case:

$$E = \sum_{i=1}^{3}\alpha_i A_i - V \tag{11}$$

Now we consider a variation of the position of vertex p in the form:

$$\mathbf{p}(t) = \mathbf{p} + t\mathbf{v}_p + O(t^2), \quad \mathbf{v}_p \in \mathbb{R}^3, \ |t| \ll 1 \tag{12}$$

Then the first variation of E can be written in the form:

$$\delta E(\mathbf{v}) = \left.\frac{d}{dt}\right|_{t=0} E = \sum_p \langle \nabla E(p), \mathbf{v}_p \rangle \tag{13}$$

where the energy gradient $\nabla E(p)$ for each vertex p is given as follows:

1. For each interior vertex p of the surface M_i for $i = 1, 2$:

$$\nabla E(p) = \alpha_i \nabla A_i(p) - \nabla V(p) \tag{14}$$

where

$$\nabla A_i(p) = \frac{1}{2} \sum_{T=(p,q_j,q_{j+1}) \in \mathrm{star}\,(p)} \boldsymbol{\nu}_T \times (\mathbf{q}_{j+1} - \mathbf{q}_j) \tag{15a}$$

$$\nabla V(p) = \frac{1}{6} \sum_{T=(p,q_j,q_{j+1}) \in \mathrm{star}\,(p)} \mathbf{q}_{j+1} \times \mathbf{q}_j \tag{15b}$$

where $\mathrm{star}\,(p)$ is the vertex star of p. Therefore the stationary condition $\nabla E(p) = \mathbf{0}$ gives the discrete CMC condition introduced in Ref. (Polthier and Rossman, 2002), which corresponds to the stationary condition $1 + 2\alpha_i H_i = 0$ in the smooth case.

2. For the interior vertex p of the surface M_3, we have

$$\begin{aligned} \nabla E(p) &= \alpha_3 \nabla A_3(p) \\ &= \frac{\alpha_3}{2} \sum_{T=(p,q_j,q_{j+1}) \in \mathrm{star}\,(p)} \boldsymbol{\nu}_T \times (\mathbf{q}_{j+1} - \mathbf{q}_j) \end{aligned} \tag{16}$$

Therefore the stationary condition $\nabla E(p) = \mathbf{0}$ gives the discrete minimal condition introduced in Refs. (Polthier and Rossman, 2002; Pinkall and Polthier, 1993).

3. For each vertex p on Γ, we introduce the following notations:

$$\nabla A_i^{\mathrm{b}}(p) = \frac{1}{2} \sum_{T=(p,q_j,q_{j+1}) \in \mathrm{star}\,(p) \cap M_i} \boldsymbol{\nu}_T \times (\mathbf{q}_{j+1} - \mathbf{q}_j) \tag{17a}$$

$$\nabla V_i(p) = \frac{1}{6} \sum_{T=(p,q_j,q_{j+1}) \in \mathrm{star}\,(p) \cap M_i} \mathbf{q}_{j+1} \times \mathbf{q}_j \tag{17b}$$

where $i = 1, 2, 3$. Then the energy gradient $\nabla E(p)$ can be written as follows:

$$\nabla E(p) = \sum_{i=1}^{2} (\alpha_i \nabla A_i^{\mathrm{b}}(p) - \nabla V_i(p)) + \alpha_3 \nabla A_3^{\mathrm{b}}(p) \tag{18}$$

The stationary condition $\nabla E(p) = \mathbf{0}$ corresponds to the "contact angle condition" in the smooth case; however, we have additional terms $\nabla V_1(p)$ and $\nabla V_2(p)$ in the discrete setting.

4. For each vertex $p \in \Gamma_3 = M_3 \cap \Pi$, we only consider the variation parallel to Π; i.e.,

$$\nabla E(p) = \alpha_3 (\nabla A_3^{\mathrm{b}}(p) - \langle \nabla A_3^{\mathrm{b}}(p), \mathbf{e}_3 \rangle \mathbf{e}_3) \tag{19}$$

where $\mathbf{e}_3 = (0, 0, 1)$.

5. Vertices on $\Gamma_1 \cup \Gamma_2$ are fixed as mentioned in Sec. 2.2.

Note that the numbers 1–5 in Fig. 3 correspond to above cases 1–5.

For the case in which three or more external surfaces are connected, suppose k_1-external surfaces M_1, $M_2, \ldots, M_{k_1}$ are connected with k_2-auxiliary internal surfaces M_{k_1+1}, $M_{k_1+2}, \ldots, M_{k_1+k_2}$.

A case of $k_1 = k_2 = 3$ is shown in Fig. 4. In this setting, we consider the energy function

$$E = \sum_{i=1}^{k_1+k_2} \alpha_i A_i - V \tag{20}$$

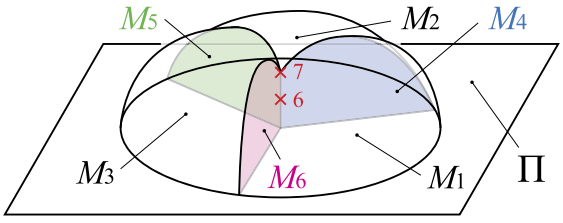

Fig. 4. Typical example of three exterior surfaces (M_1, M_2, M_3) are connected and auxiliary internal surfaces (M_4, M_5, M_6) are inserted between them.

where V is the volume bounded by $M_1, M_2, \ldots, M_{k_1}$ and the plane Π. As in the previous double bubble type setting, we can show that the stationary conditions for interior vertices of $M_1, M_2, \ldots, M_{k_1}$ give the discrete CMC conditions, those for the internal boundary between a pair of surfaces in $\{M_1, M_2, \ldots, M_{k_1}\}$ give constant angle condition, and for interior vertices of $M_{k_1+1}, M_{k_1+2}, \ldots, M_{k_1+k_2}$ give the discrete minimal condition.

Therefore it is enough to consider the gradient of E with respect to each vertex p on an intersection of some auxiliary surfaces in $\{M_{k_1+1}, M_{k_1+2}, \ldots, M_{k_1+k_2}\}$. Let $\mathcal{K}_p$ be the set of indices of surfaces including the vertex p. Then the following relations are to be satisfied:

6. For the interior vertex p along the intersection we have

$$\nabla E(p) = \sum_{i \in \mathcal{K}_p} \alpha_i \nabla A_i^{\mathrm{b}}(p) \tag{21}$$

7. For the "top" vertex on the intersection, we have

$$\nabla E(p) = \sum_{i \in \mathcal{K}_p} (\alpha_i \nabla A_i^{\mathrm{b}}(p) - \nabla V_i(p)) \tag{22}$$

2.4. Existence and uniqueness of solution

The stationary point of the energy functional is regarded as the solution satisfying P-CMC conditions. The existence of a solution cannot be generally known in advance. Still, it is possible to check a posteriori whether a solution exists by minimizing the energy functional and checking convergence to a solution satisfying stationary conditions. Since the nodal locations are unbounded in this study, convergence to a stationary point indicates that the solution exists.

Depending on a combination of hyperparameters and boundary shape, the stationary condition may not always be satisfied. Even in such cases, it is possible to improve the approximation accuracy of P-CMC by increasing the resolution of the mesh.

In terms of the uniqueness of solution, the stationary point is not a unique solution because the energy functional is generally nonconvex. The surface shape depends on the internal boundary shape that is generated through minimization of the energy functional. This also means that various shapes can be generated by varying the parameters for the movement of vertices on the internal boundary.

3. Implementation details

3.1. Workflow

Based on the discretized MCF formulated in Sec. 2.3, the overall workflow to obtain discrete P-CMC surfaces is explained in this section. The overview of the process is illustrated in Fig. 5.

The proposed algorithm requires a triangular mesh to be transformed, fixed points along boundaries of the mesh, and the values of hyper-parameters. To create an internal boundary, the input mesh needs to be divided into patches of surface called sub-meshes.

Since discrete P-CMC surfaces are difficult to obtain explicitly, an iterative procedure is adopted here. First, the MCF at each vertex is obtained by Eqs. (14)–(22). Then, the scale of the change of vertex positions, denoted as t, is obtained using a line search algorithm, which is further explained in Sec. 3.3. Once the MCF and its magnitude t are determined, vertex positions are updated introducing the Nesterov momentum, which is explained in detail in Sec. 3.2.

The above processes repeat until the energy functional is considered stationary: $\nabla E(p) \simeq \mathbf{0}$ for all the vertices.

3.2. Nesterov momentum for fast convergence

The energy function is minimized using the steepest descent approach, as follows, moving the vertex position $\mathbf{p}$ in the direction of MCF obtained in Sec. 2.3:

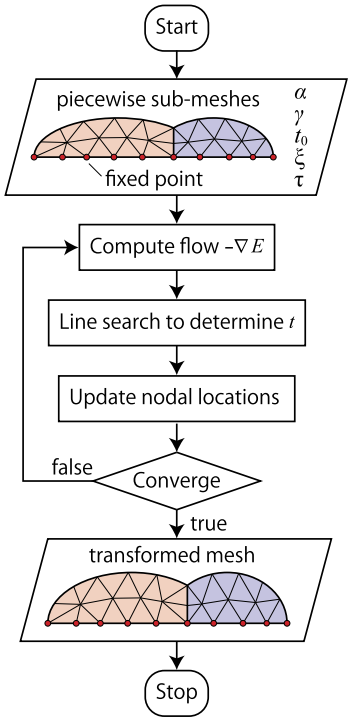

Fig. 5. Overall workflow of the proposed method.

$$\mathbf{p} \leftarrow \mathbf{p} - t\nabla E(p) \tag{23}$$

We further introduce the Nesterov momentum (Nesterov, 1983) to accelerate the convergence. Classical momentum has been known to accelerate convergence to a local minimum (Polyak, 1964), and the Nesterov momentum can be regarded as the variant of classical momentum. The methods based on Nesterov momentum can improve convergence for nonconvex optimization (Ghadimi and Lan, 2016; Paquette et al., 2018). Sutskever et al. (2013) analyzed that Nesterov momentum works more stably than classical momentum due to a quicker and more responsive way of velocity changes.

Let $\mathbf{d}$ initialize as a zero vector in the beginning of analysis, then the updating scheme of $\mathbf{P}$, positions of all vertices, introducing the Nesterov momentum simplified by Sutskever et al. (2013) is formulated as follows:

$$\mathbf{d} \leftarrow \gamma\mathbf{d} - t\nabla E(p + \gamma\mathbf{d}) \tag{24a}$$

$$\mathbf{P} \leftarrow \mathbf{P} + \mathbf{d} \tag{24b}$$

where $\gamma \in (0, 1)$ is a constant to adjust the momentum. In the next subsection, the adjustment method of t is explained.

3.3. Line search

When updating the vertex positions using the MCF, the solution will diverge or unnecessarily many iterations will be performed unless the magnitude of update of vertex positions in the direction of MCF is appropriately assigned. To address this problem, a line search scheme is adopted in determining the value of t.

Line search methods are general approaches to find the minimum/maximum of a nonlinear function by determining a direction vector and a step size at each step of iterations of nonlinear optimization. Since the direction vector is equivalent to $-\nabla E$, determining the step size only is the purpose of employing the line search scheme.

A line search algorithm using the Armijo condition is already adopted for the energy minimization problem of discrete surfaces (Hayashi et al., 2021; Tellier et al., 2018), and a similar algorithm is adopted here. Let $E(\tilde{\mathbf{P}})$ denote the energy functional value associated with the vector $\tilde{\mathbf{P}}$ consisting of positions of all vertices except those on the fixed boundaries. Then the Armijo condition that the step size t should meet is defined as (Ninomiya, 2017)

$$E(\tilde{\mathbf{P}} - t\nabla E + \gamma\mathbf{d}) \leq E(\tilde{\mathbf{P}} + \gamma\mathbf{d}) + \xi t\|\nabla E(\tilde{\mathbf{P}} - t\nabla E + \gamma\mathbf{d})\|^2 \tag{25}$$

where $\xi \in (0, 1)$ is a constant to determine the acceptance threshold of t.

To obtain a larger value of t that satisfies the Armijo condition (25), t starts from a sufficiently large value t_0 and is multiplied by another constant $\tau \in (0, 1)$ until the Armijo condition is satisfied. However, since there are cases where no positive t satisfies the Armijo condition due to local surface irregularity, $t_0\tau^5$ is set as the lower limit of t.

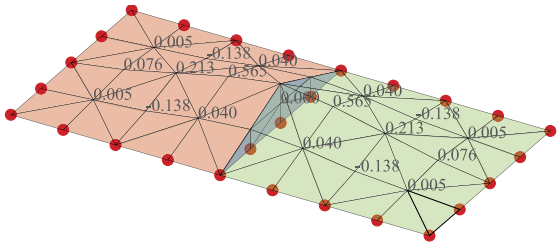

Fig. 6. Initial shape of Example 1. (For interpretation of the colors in the figure(s), the reader is referred to the web version of this article.)

3.4. Hyper-parameter assignment

The values of α for external patches can be determined based on the target mean curvature $\bar{H}$, because the relationship $\bar{H} = -1/(2\alpha)$ holds between α and $\bar{H}$. However, specifying unreasonable mean curvatures causes divergence. This also means that it is important to properly set the positions of fixed points in order to achieve the target mean curvature.

The value of α for auxiliary patch determines the shape at the internal boundary. Note that the value of α for the auxiliary patch induces the opposite effect onto the external patches around the internal boundary as expressed in Eq. (7); i.e., smaller α for the auxiliary patch makes the external patches connect more smoothly. If the values of α are the same for the two patches connected to the internal boundary, then the patches are expected to intersect with the same angle with the auxiliary patch.

The parameter γ in the Nesterov momentum determines the behavior of the shape variation during iterations, and its careful adjustment is necessary to ensure fast convergence. In this study, γ is set to be 0.9.

Even though the line search scheme is employed to automatically adjust the magnitude of vertex movement, the initial step size t_0 significantly affects the efficiency and the stability of the algorithm; if t_0 is large, the mesh can reach a stationary point in fewer iterations while the risk of divergence increases; if t_0 is small, the shape is less likely to diverge, but the algorithm requires more iterations to converge. If the mesh has good properties, i.e., the edge lengths are almost the same, setting t_0 to a value in the range $[0.01, 0.1]$ empirically achieves both efficiency and stability.

The values of ξ and τ are less important compared with the above parameters. However, assigning large values to ξ and τ may cause redundant line search iterations to satisfy the convergence criterion: $\nabla E(p) \simeq \mathbf{0}$ for vertices free to move. $\xi = 0.2$ and $\tau = 0.5$ are adopted in this study.

4. Numerical examples

Several P-CMC surfaces are generated using the proposed method. The units are omitted because they are not important to describe the methodology. The computational cost and the quality of the obtained shapes are discussed.

To verify that the converged shape has a CMC property, the mean curvature at the interior vertices of the surfaces are evaluated based on the discrete Laplace-Beltrami operator (Meyer et al., 2002) in the following; note that the barycentric area is utilized for computing the area around each vertex in the operator.

4.1. Example 1: two square patches

The first example is a very simple mesh composed of two external patches and an auxiliary patch between them, as shown in Fig. 6. Each external patch has a 4×4 square plan, and the patch is further divided into grids with a square plane with a side length of 1. Vertices whose positions are to be fixed during the shape variation are indicated in red. The initial shape is assigned so that the height of the vertex at the center of the internal boundary is 1.0, and the height of each vertex is set smoothly so that the height becomes 0 toward the fixed vertex.

The numbers in Fig. 6 represent the mean curvature of the vertices inside the patches. The target mean curvature is 0.25; accordingly, α is set as 2.0 for the both external patches. t_0 is set as 0.005 unless otherwise specified.

First, the relationship between α for the auxiliary patch and the resulting shape is discussed. Fig. 7 illustrates the elevations of the initial shape and the resulting shapes with different α for the auxiliary patch after 300 iterations. It is confirmed from the results in this figure that the value of α for the auxiliary patch has a significant effect on the shape of the internal boundary; the smaller α is, the more smoothly the two external patches connect, and the larger α is, the greater the change in tangent direction at the connection.

The diagonal view of Fig. 7(d) is shown in Fig. 8. The numbers in this figure represent the mean curvature of each internal vertex. In this example, the final shape does not strictly satisfy the specified mean curvature condition. The degree of coincidence of the mean curvature of the resulting shape with the specified value depends on the boundary condition and the roughness of the mesh. When the number of mesh elements is increased to four times with the same shape, the error from the specified mean curvature becomes smaller as shown in Fig. 9. Note that the same hyper-parameters are used for the both meshes.

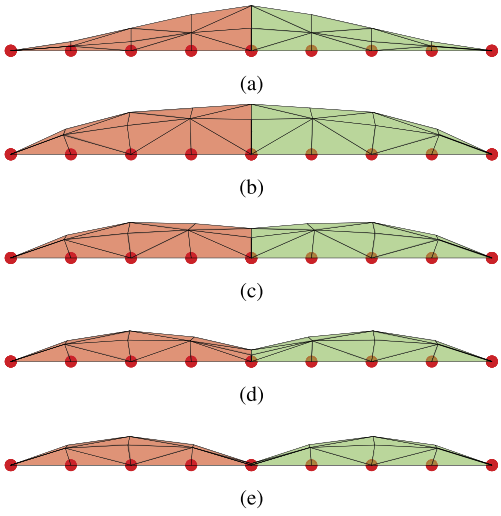

Fig. 7. Elevations of Example 1. (a) Initial shape. (b-e) Final shape with different α for the auxiliary patch; (b) $\alpha = 0.0$, (c) $\alpha = 1.0$, (d) $\alpha = 2.0$, (e) $\alpha = 3.0$.

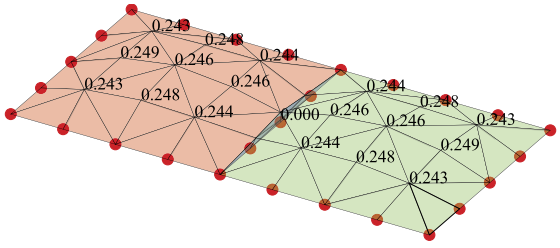

Fig. 8. Final shape of Example 1.

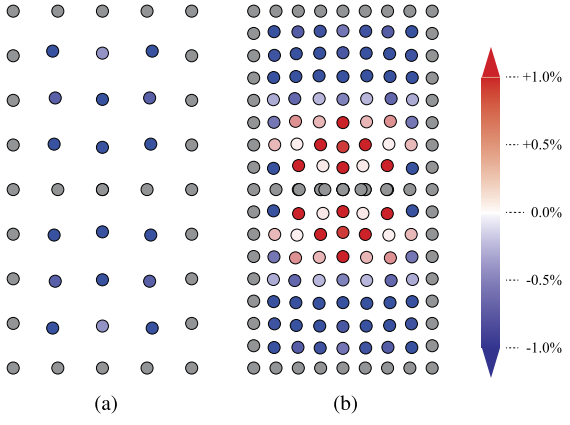

Fig. 9. Error between the mean curvatures of the transformed shape and their target values of Example 1. (a) Coarse mesh. (b) Fine mesh.

Next, the contributions of the Nesterov momentum and line search are discussed. Here, α for the auxiliary patch is fixed as 2.0, and t_0 is set as 0.05, which is larger than the default setting to clarify the difference in the results with and without the Nesterov momentum and line search. Fig. 10 describes the histories of the energy functional value for 300 steps. The blue and green lines are the histories when the Nesterov momentum is not used, and the slopes of the energy decrease can still be seen in the second half of iterations, compared with the proposed method (black line). This result indicates that the proposed method accelerates convergence. From the black and red lines, the line search can improve the stability when used in combination with Nesterov momentum; the oscillation of the energy functional by Nesterov momentum can be alleviated by the line search.

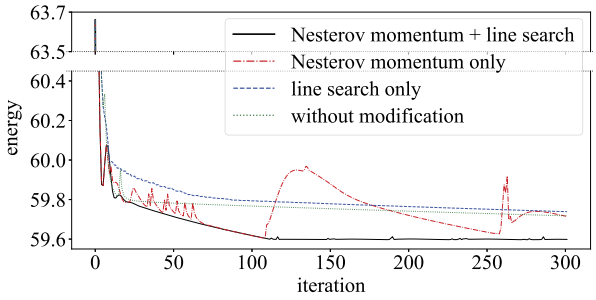

Fig. 10. Histories of energy functional value of Example 1.

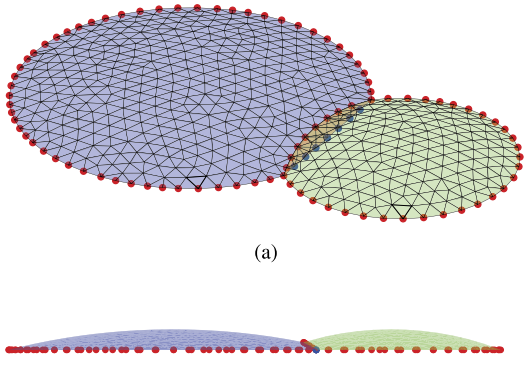

Fig. 11. Initial shape of Example 2. (a) Diagonal view. (b) Elevation view.

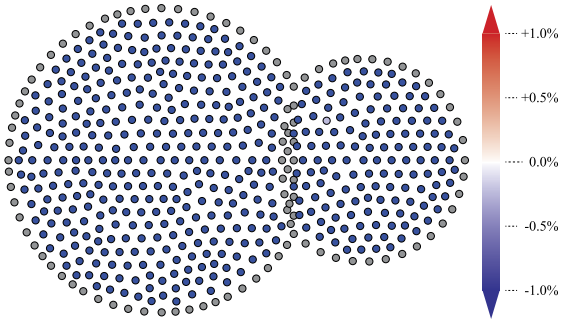

Fig. 12. Error between the mean curvatures of the initial shape and their target values of Example 2.

4.2. Example 2: two circular patches

Different target mean curvatures are assigned in this example. Consider a mesh consisting of two circular external patches and an auxiliary patch between them, as shown in Fig. 11. The larger external patch is a discretized region of $Z \geq 0$ of a sphere with a center point $(-5.0, 0.0, -17.5)$ and a radius of 18.5; i.e., the initial mean curvature is approximately 0.054. The smaller external patch is a discretized region of $Z \geq 0$ of a sphere with a center point $(3.0, 0.0, -7.5)$ and a radius of 8.5; i.e., the initial mean curvature is approximately 0.118. The target mean curvature is 0.125 for the larger patch and 0.167 for the smaller patch; accordingly, $\alpha = 4.0$ and $\alpha = 3.0$ for the external patches, respectively. In this example, the value of α for the auxiliary patch is set as 4.0, and t_0 is 0.01. The positions of vertices on the external boundaries are fixed, as highlighted in red. The vertices on the bottom boundary of the auxiliary patch are vertically fixed, as highlighted in blue. Fig. 12 shows the error between the mean curvatures of the initial shape and their target values.

Fig. 13 shows the final geometry obtained by the proposed method. As clearly seen in Fig. 13(b), a more convex shape is obtained by specifying large mean curvatures. The errors at interior vertices on the external patches are illustrated in Fig. 14; the final shape converges to the specified mean curvatures with high accuracy.

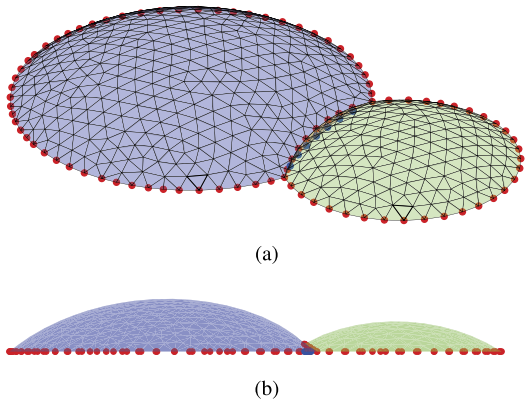

Fig. 13. Final shape of Example 2. (a) Diagonal view. (b) Elevation view.

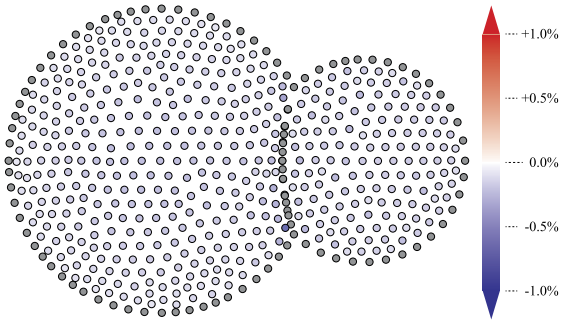

Fig. 14. Error between the mean curvatures of the transformed shape and their target values of Example 2.

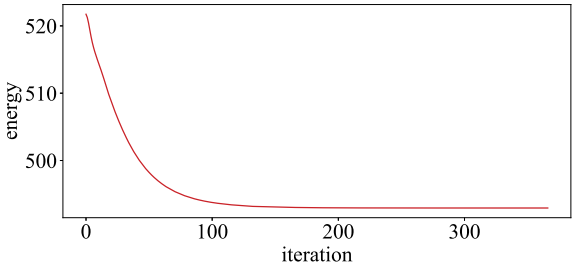

Fig. 15. History of energy functional value of Example 2.

The history of the energy functional through the iterations is plotted in Fig. 15. The energy functional has been smoothly minimized, which implies the stability of the proposed method. The squared sum of the elements in ∇E is 12.204 at the beginning of iterations, and the value is reduced to less than 1.0×10^{-4} at the last iteration.

Next, the convergence property depending on α is further investigated. Fig. 16 shows the squared sum of the elements in ∇E after 200 iterations for various combinations of α. This result shows that α is a crucial parameter on the convergence property.

Regarding α of the auxiliary patch, there is no adverse effect on convergence if α is small. On the other hand, if this value is too large, the area of the auxiliary patch will approach 0, causing instability in the analysis due to shape distortion.

Regarding α of the exterior patches, well-converged solutions are obtained especially when α of the smaller patch is slightly smaller than that of the larger patch. This tendency can be intuitively understood; for an equilibrium shape subject to equal internal pressure, smaller surface have larger mean curvature, i.e., smaller α, and large surface have smaller mean curvature, i.e., larger α. The convergence property worsened when the α values assigned to the two exterior patches were too different. Furthermore, the process diverged due to over-inflation when too small α was assigned.

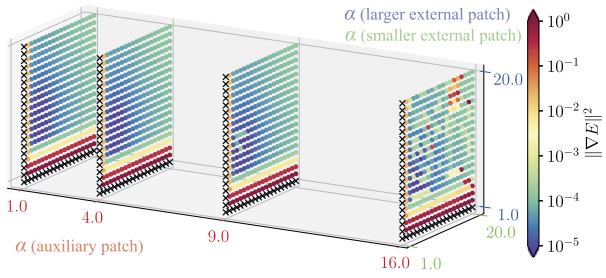

Fig. 16. Convergence property for various combinations of α in Ex.2. Note that $\times$ indicates that the analysis failed due to divergence.

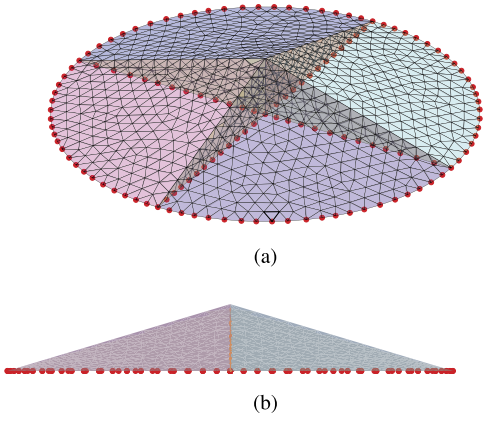

Fig. 17. Initial shape of Example 3. (a) Diagonal view. (b) Elevation view.

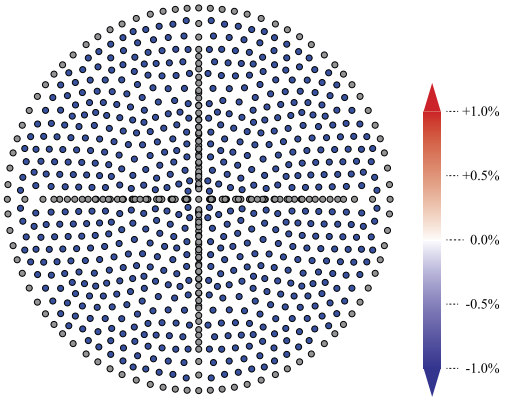

Fig. 18. Error between the mean curvatures of the initial shape and their target values of Example 3.

4.3. Example 3: four fan-shaped patches

This example contains four fan-shaped external patches and four auxiliary patches between them, as shown in Fig. 17. The combined four external patches form a circular plan with a radius of 20. Each auxiliary patch is a right triangle with a base of 20 and a height of 8, and the auxiliary patches share the vertical side. The values of α for auxiliary patches are 3.0, and those for external patches are 10.0; i.e., the target mean curvatures are 0.05. The locations of boundary vertices highlighted in red are fixed. The value of t_0 is 0.01 in this example. Fig. 18 shows the error between the mean curvatures of the initial shape and their target values.

Fig. 19 shows the final geometry obtained by the proposed method. A bulging shape like pneumatic membrane structure is obtained through the MCFs. The shape of the auxiliary patches changes from a right triangle to an elliptical segment. On the other hand, the intersection of the four auxiliary patches retain the original vertical line, even though the algorithm did not constrain the positions of the internal vertices. The errors at interior vertices on the external patches are successfully reduced to zero, as illustrated in Fig. 20.

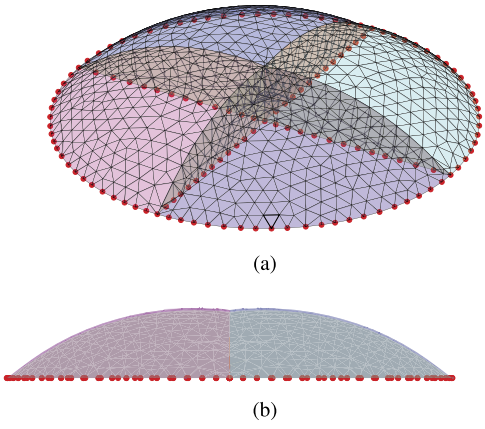

Fig. 19. Final shape of Example 3. (a) Diagonal view. (b) Elevation view.

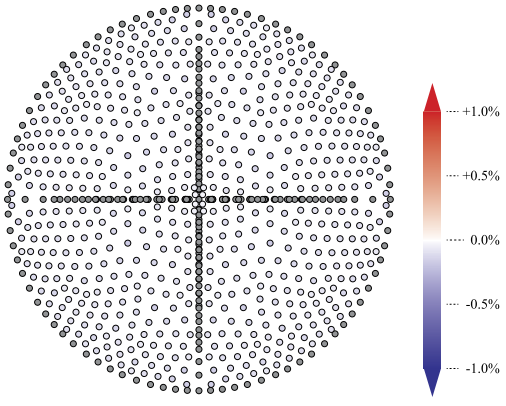

Fig. 20. Error between the mean curvatures of the transformed shape and their target values of Example 3.

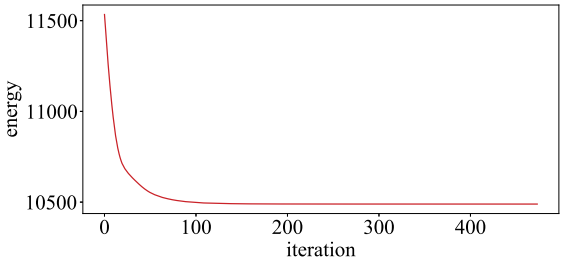

Fig. 21. History of energy functional value of Example 3.

The energy functional has been almost monotonically reduced through the iterations as plotted in Fig. 21. The squared sum of the elements in ∇E is 7893.633 at the first iteration, and the value is reduced to below 0.005 at the last iteration. From these results, it has been confirmed that the proposed method works well even when more than two external patches intersect.

4.4. Example 4: non-planar internal and external boundaries

To investigate the applicability of the proposed method to irregular shapes, the proposed method is applied to a more complex discrete surface as shown in Fig. 22. Although this surface simply consists of three external patches and two auxiliary patches between them, this example differs from the other examples in that the interior and external boundaries have non-planar shapes and that the middle external patch have a hole. The initial boundary shapes are generated by Bézier curves. The overall shape is defined within the bounding box of $(width, depth, height) = (190.22, 101.56, 29.17)$. The maximum time step is set as $t_0 = 0.005$, and the values of α are 30.0 for the external patches, 10.0 for the left auxiliary patch, and 15.0 for the right auxiliary patch, respectively. Note that the bottom edges of the auxiliary patches are fixed to

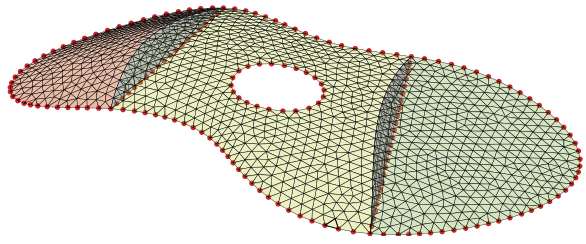

(a)

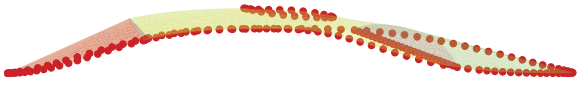

(b)

Fig. 22. Initial shape of Example 4. (a) Diagonal view. (b) Elevation view.

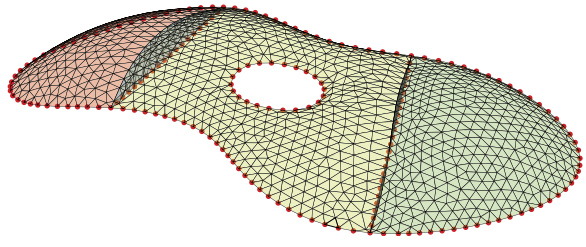

(a)

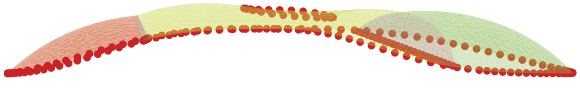

(b)

Fig. 23. Final shape of Example 4. (a) Diagonal view. (b) Elevation view.

move in all directions because the bottom edges are sloped in the height direction; i.e., the bottom nodes of the auxiliary patches move toward the lower end to minimize its surface area if they are free to move horizontally. The squared sum of the elements ∇E for the initial shape is 2.678×10^5.

The resulting shape after 225 iterations, which has the least maximum error among 1000 iterations, is shown in Fig. 23. As a consequence of relatively small α, the area has been increased due to small in-plane tension. There are still some errors between the discrete mean curvatures and their target values, especially around the external boundaries as shown in Fig. 24; however, the largest error is only 0.73%, which demonstrates that a swollen shape approximating the specified mean curvatures can be obtained.

Although the energy functional seems to have converged according to Fig. 25, the squared sum of the elements in ∇E after 225 iterations is still a non-negligible value of 0.874, and it has slightly reduced to 0.596 after 500 iterations. Note that further iterations did not produce significant impact in the result; the squared sum of the elements in ∇E after 1000 iterations is 0.572, and the largest error to the specified mean curvature did not improve anymore.

5. Conclusions

In this study, we proposed a method to obtain P-CMC discrete surfaces by the MCF. The internal boundary between patches, or sub-meshes, is C^0 continuous, and the patches can have different target mean curvatures.

A continuous form of energy functional is first formulated for a surface with two external patches so that its Euler-Lagrange equation corresponds to the conditions of P-CMC. Thus, a continuous form of MCF is derived for obtaining P-CMC surface. The functional is then discretized into an energy function using a polygonal surface of triangular meshes. The discretized form of MCF is derived as the negative gradient flow of the function with respect to the positions of vertices inside the surface patches and their internal boundaries; accordingly, the shapes of surface patches and the internal boundaries can be integrally generated using the MCF.

By defining the MCF as the negative gradient flow of an energy function, the problem of generating a P-CMC surface is regarded as a minimization problem of an energy function, and various sophisticated methods of nonlinear optimization can

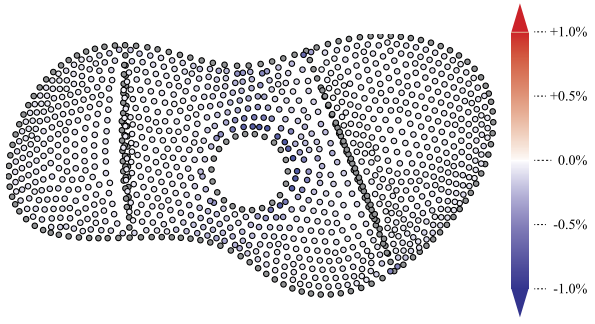

Fig. 24. Error between the mean curvatures of the transformed shape and their target values of Example 4.

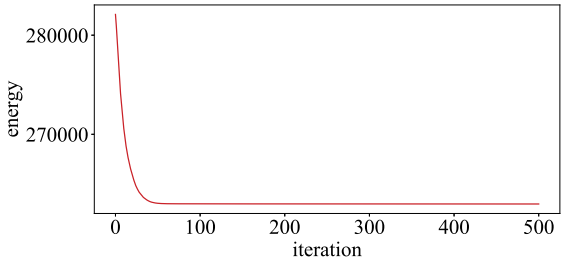

Fig. 25. History of energy functional value of Example 4.

be utilized. Because the problem of generating P-CMC surfaces is formulated as an unconstrained nonlinear programming problem, a simple steepest descent algorithm can be used. To accelerate convergence and stabilize the algorithm, a line search scheme and the Nesterov momentum are employed. Through Example 1, these modifications are found to be effective; introducing Nesterov momentum successfully accelerated convergence, and the line search alleviated the oscillation of the energy function caused by the Nesterov momentum.

In Example 2, the proposed method was successfully applied to the case where different target mean curvatures are assigned, and the convergence property depending on α was further investigated. In Example 3, a rational P-CMC surface was generated in which four external patches intersect at one point. In Example 4, the proposed method was applied to a complicated shape with non-planar internal and external boundaries, and the resulting shape approximated the target mean curvatures despite not fully converging. Although convergence depends largely on the mesh resolution and boundary shapes, the solutions approximated P-CMC with high accuracy, demonstrating that the proposed method is a useful tool for generating P-CMC discrete surfaces.

We also provided guidance on setting hyper-parameters required when implementing the proposed method. In particular, the value of α assigned to each auxiliary patch plays an important role in determining the final shape; the external patches will connect smoothly when α of the auxiliary patch is small, and the change in tangent direction of the surface at the connection will be large when α of the auxiliary patch is large. This is because α is equivalent to the magnitude of tensile force when the surface patches are at equilibrium with uniform tensile forces against the internal pressure.

In general design cases of architectural structures, the boundary shape is determined by design requirements. Meanwhile, in the proposed method, an appropriate set of α values and boundary shapes needs to be explored to find a preferable shape. In addition, the accuracy for approximating the target mean curvature highly depends on the initial surface shape, especially around the external and internal boundaries. Therefore, the proposed approach requires a trial-and-error process to improve the quality of the solution, which may be a limitation of the method. Besides, the locations of internal boundaries on the surface and on the plane need to be specified by providing auxiliary surfaces in advance, which is also time-consuming.

In order to apply this method to more general cases, not just architectural design, the uncontrollability of element shapes may be another limitation. Since the method iteratively modifies nodal positions in their normal direction without constraining their tangential movement, the flows are prone to tangential distortion, which degrades element shapes and may cause numerical instability. Still, tangential distortion can be alleviated by providing near-equilateral mesh as an initial shape. Although there are several approaches to mesh rationalization through energy minimization (Crane et al., 2013; Vidal et al., 2012), managing both p-CMC and mesh quality is still an open problem.

CRediT authorship contribution statement

Kazuki Hayashi: Software, Visualization, Writing – original draft. **Yoshiki Jikumaru:** Conceptualization, Methodology, Writing – original draft. **Makoto Ohsaki:** Project administration, Validation, Writing – review & editing. **Takashi Kagaya:** Conceptualization, Methodology, Writing – original draft. **Yohei Yokosuka:** Validation, Writing – review & editing.

Declaration of competing interest

The authors declare that they have no known competing financial interests or personal relationships that could have appeared to influence the work reported in this paper.

Data availability

Data will be made available on request.

Acknowledgements

This study is supported by JST CREST Grant No. JPMJCR1911. Valuable comments from Prof. Kenji Kajiwara at Institute of Mathematics for Industry, Kyushu University are appreciated.

References

Arora, S., Tae-Hee, Lee, Cardoso, J.B., 1992. Structural shape sensitivity analysis: relationship between material derivative and control volume approaches. AIAA J. 30 (6).
Brakke, Kenneth A., 1978. The Motion of a Surface by Its Mean Curvature (MN-20). Princeton University Press, Princeton, NJ, USA.
Brakke, Kenneth A., 1992. The surface evolver. Exp. Math. 1 (2), 141–165.
Burger, Noah, Billington, David P., 2006. Felix Candela, elegance and endurance: an examination of the Xochimilco shell. J. Int. Assoc. Shell Spat. Struct. 47 (3), 271–278.
Cao, Xin, Xu, Dongpo, Yao, Yuan, Han, Lu, Terasaki, Osamu, Che, Shunai, 2016. Interconversion of triply periodic constant mean curvature surface structures: from double diamond to single gyroid. Chem. Mater. 28 (11), 3691–3702.
Cottrell, J. Austin, Hughes, Thomas J.R., Bazilevs, Yuri, 2009. Isogeometric Analysis: Toward Integration of CAD and FEA. John Wiley & Sons, Hoboken, NJ, USA.
Crane, Keenan, Pinkall, Ulrich, Schröder, Peter, 2013. Robust fairing via conformal curvature flow. ACM Trans. Graph. 32 (4).
Cui, Jinglan, Ohsaki, Makoto, 2018. Shape design of curved surface of membrane structure using developable surface. J. Int. Assoc. Shell Spat. Struct. 59 (3), 199–214.
Desbrun, Mathieu, Meyer, Mark, Schröder, Peter, Barr, Alan H., 1999. Implicit fairing of irregular meshes using diffusion and curvature flow. In: Proceedings of the 26th Annual Conference on Computer Graphics and Interactive Techniques, SIGGRAPH '99. NY, USA, pp. 317–324.
Farin, Gerald, 2001. Curves and Surfaces for CAGD: A Practical Guide, 5th edition. Morgan Kaufmann Publishers Inc., San Francisco, CA, USA.
Fujita, Shinnosuke, Ohsaki, Makoto, 2010. Shape optimization of free-form shells using invariants of parametric surface. Int. J. Space Struct. 25 (3).
Gao, Yuliang, Guo, Yujie, Zheng, Shijie, 2019. A NURBS-based finite cell method for structural topology optimization under geometric constraints. Comput. Aided Geom. Des. 72, 1–18.
Ghadimi, Saeed, Lan, Guanghui, 2016. Accelerated gradient methods for nonconvex nonlinear and stochastic programming. Math. Program. 156, 59–99.
Hayashi, Kazuki, Jikumaru, Yoshiki, Ohsaki, Makoto, Kagaya, Takashi, Yokosuka, Yohei, 2021. Discrete Gaussian curvature flow for piecewise constant Gaussian curvature surface. Comput. Aided Des. 134, 102992.
Huisken, Gerhard, 1984. Flow by mean curvature of convex surfaces into spheres. J. Differ. Geom. 20 (1), 237–266.
Kimura, Toshiaki, Ohmori, Hiroshi, 2008. Computational morphogenesis of free form shells. J. Int. Assoc. Shell Spat. Struct. 49 (3), 175–180.
Lewis, Wanda J., Gosling, Peter D., 1993. Stable minimal surfaces in form-finding of lightweight tension structures. Int. J. Space Struct. 8 (3), 149–166.
López, Rafael, 2013. Constant Mean Curvature Surfaces with Boundary. Springer, Berlin, Heidelberg, Germany.
Mantegazza, Carlo, 2011. Lecture Notes on Mean Curvature Flow. Springer, Basel, Switzerland.
Meeks, William H., Pérez, Joaquín, 2011. The classical theory of minimal surfaces. Bull. Am. Math. Soc. 48 (3), 325–407.
Meyer, Mark, Desbrun, Mathieu, Schröder, Peter, Barr, Alan H., 2002. Discrete differential-geometry operators for triangulated 2-manifolds. In: Hege, Hans-Christian, Polthier, Konrad (Eds.), Third International Workshop "Visualization and Mathematics (VisMath)". Berlin, Germany.
Michiels, Tim, Garlock, Maria Eugenia Moreyra, Adriaenssens, Sigrid M., 2016. Seismic assessment of Félix Candela's concrete shells and their behavior during the 1985 Mexico city earthquake. A case study on the church of our lady of the miraculous medal. In: Proceedings of the 10th International Conference on Structural Analysis of Historical Constructions (SAHC2016). Leuven, Belgium, pp. 1544–1550.
Nesterov, Yurii, 1983. A method for solving a convex programming problem with convergence rate $o(1/k^2)$. Sov. Math. Dokl. 27, 372–376.
Ninomiya, Hiroshi, 2017. A novel quasi-Newton-based optimization for neural network training incorporating Nesterov's accelerated gradient. Nonlinear Theory Appl., IEICE 8 (4), 289–301.
Pan, Hao, Choi, Yi-King, Liu, Yang, Hu, Wenchao, Du, Qiang, Polthier, Konrad, Zhang, Caiming, Wang, Wenping, 2012. Robust modeling of constant mean curvature surfaces. ACM Trans. Graph. 31 (85).
Paquette, Courtney, Lin, Hongzhou, Drusvyatskiy, Dmitriy, Mairal, Julien, Harchaoui, Zaid, 2018. Catalyst for gradient-based nonconvex optimization. In: Proceedings of the 21st International Conference on Artificial Intelligence and Statistics (AISTATS), vol. 84. Lanzarote, Spain.
Pinkall, Ulrich, Polthier, Konrad, 1993. Computing discrete minimal surfaces and their conjugates. Exp. Math. 2 (1), 15–36.
Polthier, Konrad, Rossman, Wayne, 2002. Discrete constant mean curvature surfaces and their index. J. Reine Angew. Math. 2002 (549), 47–77.
Polyak, B.T., 1964. Some methods of speeding up the convergence of iteration methods. USSR Comput. Math. Math. Phys. 4 (5), 1–17.
Schneider, Robert, Kobbelt, Leif, 2001. Geometric fairing of irregular meshes for free-form surface design. Comput. Aided Geom. Des. 18 (4), 359–379.
Sutskever, Ilya, Martens, James, Dahl, George, Hinton, Geoffrey, 2013. On the importance of initialization and momentum in deep learning. In: Proceedings of the 30th International Conference on Machine Learning. Atlanta, Georgia, USA, pp. 1139–1147.
Tellier, Xavier, Hauswirth, Laurent, Douthe, Cyril, Baverel, Olivier, 2018. Discrete CMC surfaces for doubly-curved building envelopes. In: Proceedings of Advances in Architectural Geometry (AAG2018). Göteborg, Sweden, pp. 166–193.

Thomas, Edwin L., Anderson, David M., Henkee, Chris S., Hoffman, David, 1988. Periodic area-minimizing surfaces in block copolymers. Nature 334 (6183), 598–601.
Vidal, Vincent, Wolf, Christian, Dupont, Florent, 2012. Combinatorial mesh optimization. Vis. Comput. 28 (5), 511–525.
Yu, Yang, Wu, Qingbiao, Khan, Yasir, 2015. Constructing constant mean curvature surfaces with fixed-point half dynamic model. Neural Comput. Appl. 27, 2577–2586.
Zolésio, Jean-Paul, 1981. The material derivative (or speed) method for shape optimization. In: Haug, Edward J., Cea, Jean (Eds.), Optimization of Distributed Parameter Structures. Sijthoff & Nordhoff, Iowa, USA, pp. 1089–1151.